Journal of Zhejiang University SCIENCE A
ISSN 1009-3095
http://www.zju.edu.cn/jzus
E-mail: jzus@zju.edu.cn

Precise navigation for a 4WS mobile robot

HE Bo (何 波)

(*School of Information Science and Engineering, Ocean University of China, Qingdao 266071, China*)

E-mail: bhe@ouc.edu.cn

Received Jan. 18, 2005; revision accepted July 10, 2005

Abstract: Position and orientation estimation with high accuracy based on GPS and encoders for a four-wheel-steering vehicle (4WS) mobile robot is presented. A GPS receiver working in Real-Time Kinematics (RTK) mode can offer centimeter-level accuracy for our vehicle. In addition to GPS, the vehicle is equipped with four incremental encoders and two absolute encoders to provide information on wheels for estimation of velocity and sideslip angle of vehicle. The proposed architecture of position and orientation estimation consists of two extended Kalman filters and a processing unit of Runga-Kutta based dead reckoning. The first EKF fuses data from six encoders to estimate the vehicle velocity and the sideslip angle. The second EKF is applied to the estimation of position and orientation based on the measurement from precise RTK GPS data and output from first EKF. To obtain higher accuracy of estimation, an arbitrator is designed to switch between EKF2 and dead reckoning. The results and analysis of experiments are presented to show the effectiveness of the proposed approach. Limitations of the proposed approach and future works are also pointed out and discussed in this paper.

Key words: Extended Kalman filter, Navigation, Dead reckoning, GPS
doi:10.1631/jzus.2006.A0185 **Document code:** A **CLC number:** TP24

INTRODUCTION

Precise navigation is being researched and applied in various fields, especially for outdoor mobile robots (Wang *et al*., 1998; Lee, 1997; Iida *et al*., 2000), such as those used in cargo container transportation at seaport, in precision agriculture, military vehicles, etc. As we know, applied sensors and relevant data processing basically determine the accuracy of navigation. In our research, GPS and encoders are used as navigation sensors. As an absolute positioning sensor, GPS has been commercially applied in vehicles localization and navigation as well as in military areas. A GPS receiver working in Real-Time Kinematics mode can offer centimeter-level accuracy for our vehicle. In addition to GPS, the vehicle is equipped with four incremental encoders and two absolute encoders to provide information on wheels for estimation of vehicle velocity and sideslip angle. To estimate position and orientation on the basis of GPS data and encoder data, a novel architecture of position and orientation estimate is proposed, which consists of two extended Kalman filters and a processing unit of Runga-Kutta based dead reckoning. The first EKF fuses data from six encoders to estimate the velocity and sideslip angle at a reference point of the vehicle. The second EKF estimates position and orientation based on the measurement from GPS data and output from the first EKF. Further, to obtain better accuracy of estimation, a dedicated arbitrator is designed to switch on or off appropriate processing unit (EKF2 or dead reckoning). The results and analysis of experiments are presented to show the effectiveness of the proposed approach.

This paper is organized as follows. Section 2 describes our research platform, a 4WS vehicle, and its kinematics model. Section 3 analyzes position and orientation estimation in detail, including the architecture of data fusion, estimation algorithms, and arbitration. Results and analysis of some experiments are provided in Section 4. Finally limitations of the proposed approach are discussed and conclusions are

presented in Section 5 and Section 6 respectively.

KINEMATICS MODEL OF A MOBILE ROBOT

Our research platform, Cycab, is a computer-aided and DC-motor-driven four wheel steering vehicle. The kinematic model used in this paper is based on the one in (Wang *et al*., 1998) that was derived for a 4WS vehicle. The motion of the vehicle can be described in global coordinates by using the "bicycle model" (Tay, 1999) as illustrated in Fig.1. The reference point *CG* is chosen at the center of gravity of the vehicle. Point *O* is the Instant Center of Turn. δ_f and δ_r are the steering angles of front and rear wheels. (x, y, ψ) defines the configuration of the vehicle body, where, (x, y) is the position of the reference point in global coordinates and ψ is the vehicle heading angle.

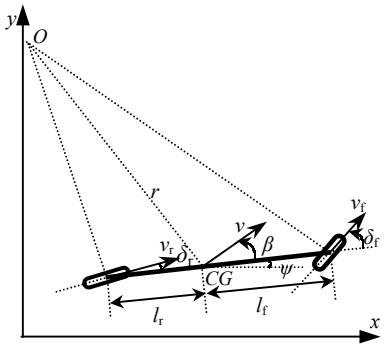

Fig.1 Kinematics model

The kinematic model can be derived based on principles of geometry as follows:

$$\begin{aligned} x(k+1) &= x(k) + \Delta v(k)\cos[\psi(k)+\beta(k)], \\ y(k+1) &= y(k) + \Delta v(k)\sin[\psi(k)+\beta(k)], \\ \psi(k+1) &= \psi(k) + \Delta\frac{v(k)}{l_r\cos\delta_r}\sin[\beta(k)-\delta_r], \end{aligned} \tag{1}$$

where, Δ is the sampling interval.

POSITION AND ORIENTATION ESTIMATE WITH HIGH ACCURACY

Position and orientation estimation aims to produce the vehicle configuration, (x, y, ψ), using the measurement data from GPS and encoders mounted on the steering and driving systems.

Architecture

When reception is good, GPS measurements provide the vehicle position (x, y), but not the vehicle heading-angle. However, GPS signals are not available at all times; thus navigation requires more than the GPS. Encoders are common type of sensors in the industry. They are used to record the speed or relative position of a rotating shaft. To estimate the configuration of a vehicle, encoders are not reliable because of accumulation of error over time-drift.

As such, combination of the absolute sensors, e.g., GPS or compass and relative sensors, e.g., encoder, gyroscope and accelerometer is a natural solution (Kobayashi and Watanabe, 1994; Abbott and Powell, 1999). In this paper, we propose architecture for estimating the configuration of the vehicle based on extended Kalman filtering and Runga-Kutta method as illustrated in Fig.2. In this architecture, two extended Kalman filters are deployed; one (EKF1) is used to estimate the velocity and sideslip angle of the vehicle measuring wheels velocity and steering angle. Another one (EKF2) is used to fuse absolute positioning information from GPS and the output of the first extended Kalman filter to estimate the configuration of the vehicle, i.e., (x, y, ψ). A block of R-K is referred to as dead reckoning based on Runga-Kutta method. An arbitrator and its two virtual switches in this architecture, determine which of the estimate solutions is on service. The details of the above mentioned blocks of algorithms will be presented in the next sub-sections.

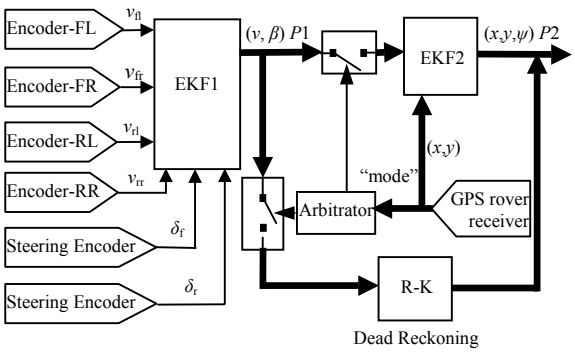

Fig.2 Architecture of position and orientation estimation

Wheel velocities v_{fl}, v_{fr}, v_{rl} and v_{rr}, are obtained from incremental encoders mounted at each of four wheels. δ_{f} and δ_{r} are steering angles of two front wheels and two rear wheels respectively, which are measured by two absolute encoders installed at the hydraulic jacks on the vehicle.

Estimation algorithms

EKF1 estimates the vehicle velocity, v, and vehicle sideslip angle, β. It is always first choice to see if we can obtain any direct relationships from existing equations, like Eq.(1), which relates the vehicle position and orientation to the velocity and sideslip angle. Is it possible to get an explicit definition of velocity v and sideslip angle β from the vehicle position and orientation as shown in Eq.(2)?

$$v(k)=\frac{[\psi(k+1)-\psi(k)]l_{\mathrm{r}}\cos\delta_{\mathrm{r}}}{\Delta\sin\left\{\arctan\left[\dfrac{y(k+1)-y(k)}{x(k+1)-x(k)}\right]-\psi(k)-\delta_{\mathrm{r}}\right\}},$$
$$\beta(k)=\arctan\left[\frac{y(k+1)-y(k)}{x(k+1)-x(k)}\right]-\psi(k). \tag{2}$$

But obviously the vehicle orientation on the right side of the above equations is not available. So, we must explore other way to estimate v and β.

Now, let us take $[v, \beta, \rho]^{\mathrm{T}}$ as state vector x, ρ is the curvature at the center of gravity of the vehicle. Assuming that the velocity and sideslip angle of the vehicle keep constant within one sampling interval, the process model is as follows:

$$\begin{aligned} v(k+1)&=v(k)+w_v(k),\\ \beta(k+1)&=\beta(k)+w_\beta(k),\\ \rho(k+1)&=\rho(k)+w_\rho(k). \end{aligned} \tag{3}$$

$[w_v, w_\beta, w_\rho]^{\mathrm{T}}$ is process error vector, a zero-mean white noise with $\boldsymbol{Q}1$ covariance matrix. The above assumption is valid while the vehicle is driven smoothly without sharply accelerating or decelerating or turning.

The measurement model should be the equations that express the relationships between four wheels velocity, two steering angles and state vector $[v, \beta, \rho]^{\mathrm{T}}$. Fig.3 represents the vehicle kinematics based on four-wheels model. r is the instant radius at point CG, i.e., the reciprocal of ρ.

The velocities at the four wheels of the vehicle are as expressed in Eq.(4).

$$\begin{aligned} v_{\mathrm{fl}}&=v\cos\beta\left[1-\frac{b\rho}{\cos\beta}\tan\delta_{\mathrm{f}}\right],\quad v_{\mathrm{fr}}=v\cos\beta\left[1+\frac{b\rho}{\cos\beta}\tan\delta_{\mathrm{f}}\right],\\ v_{\mathrm{rl}}&=v\cos\beta\left[1-\frac{b\rho}{\cos\beta}\tan\delta_{\mathrm{r}}\right],\quad v_{\mathrm{rr}}=v\cos\beta\left[1+\frac{b\rho}{\cos\beta}\tan\delta_{\mathrm{r}}\right]. \end{aligned} \tag{4}$$

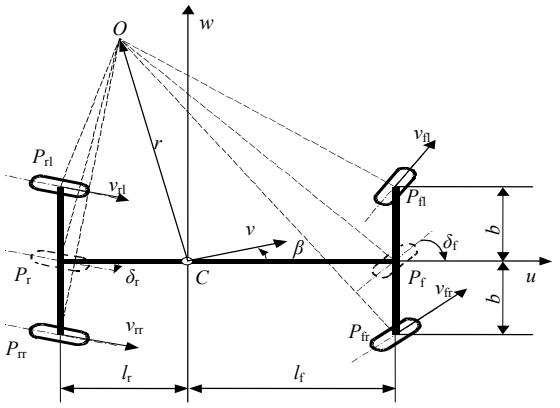

Fig.3 Kinematics model in vehicular coordinate

Taking the magnitudes only:

$$\begin{aligned} v_{\mathrm{fl}}&=v\cos\beta\sqrt{\left(1-\frac{b\rho}{\cos\beta}\right)^2+\tan^2\delta_{\mathrm{f}}},\\ v_{\mathrm{fr}}&=v\cos\beta\sqrt{\left(1+\frac{b\rho}{\cos\beta}\right)^2+\tan^2\delta_{\mathrm{f}}},\\ v_{\mathrm{rl}}&=v\cos\beta\sqrt{\left(1-\frac{b\rho}{\cos\beta}\right)^2+\tan^2\delta_{\mathrm{r}}},\\ v_{\mathrm{rr}}&=v\cos\beta\sqrt{\left(1+\frac{b\rho}{\cos\beta}\right)^2+\tan^2\delta_{\mathrm{r}}}. \end{aligned} \tag{5}$$

The front and rear steering angles δ_{f} and δ_{r} can be derived by analyzing Fig.3 and are expressed in Eq.(6).

$$\begin{aligned} \tan\frac{\delta_{\mathrm{f}}}{2}&=\frac{-\cos\beta+\sqrt{l_{\mathrm{f}}^2\rho^2+2l_{\mathrm{f}}\rho\sin\beta+1}}{l_{\mathrm{f}}\rho+\sin\beta},\\ \tan\frac{\delta_{\mathrm{r}}}{2}&=\frac{\cos\beta-\sqrt{l_{\mathrm{r}}^2\rho^2-2l_{\mathrm{r}}\rho\sin\beta+1}}{l_{\mathrm{r}}\rho-\sin\beta}. \end{aligned} \tag{6}$$

Combining Eqs.(5) and (6) yields a discretized measurement model as described by Eqs.(7) and (8).

$$\boldsymbol{z}(k)=\boldsymbol{h}1[\boldsymbol{x}(k),k]+\boldsymbol{v}(k), \tag{7}$$

$$\boldsymbol{h}1[\boldsymbol{x}(k),k]=\begin{bmatrix} v(k)\cos\beta(k)\sqrt{\left[1-\dfrac{b\rho(k)}{\cos\beta(k)}\right]^2+\left[\tan\delta_{\mathrm{f}}(k)\right]^2} \\ v(k)\cos\beta(k)\sqrt{\left[1+\dfrac{b\rho(k)}{\cos\beta(k)}\right]^2+\left[\tan\delta_{\mathrm{f}}(k)\right]^2} \\ v(k)\cos\beta(k)\sqrt{\left[1-\dfrac{b\rho(k)}{\cos\beta(k)}\right]^2+\left[\tan\delta_{\mathrm{r}}(k)\right]^2} \\ v(k)\cos\beta(k)\sqrt{\left[1+\dfrac{b\rho(k)}{\cos\beta(k)}\right]^2+\left[\tan\delta_{\mathrm{r}}(k)\right]^2} \\ \dfrac{-\cos\beta(k)+\sqrt{l_{\mathrm{f}}{}^2\rho(k)^2+2l_{\mathrm{f}}\rho(k)\sin\beta(k)+1}}{l_{\mathrm{f}}\rho(k)+\sin\beta(k)} \\ \dfrac{\cos\beta(k)-\sqrt{l_{\mathrm{r}}{}^2\rho(k)^2-2l_{\mathrm{r}}\rho(k)\sin\beta(k)+1}}{l_{\mathrm{r}}\rho(k)-\sin\beta(k)} \end{bmatrix}, \tag{8}$$

where, $\boldsymbol{z}=[v_{\mathrm{fl}}, v_{\mathrm{fr}}, v_{\mathrm{rl}}, v_{\mathrm{rr}}, \tan(\delta_{\mathrm{f}}/2), \tan(\delta_{\mathrm{r}}/2)]^{\mathrm{T}}$ is the measurement vector; $\boldsymbol{v}$ is the measurement error vector, which is a zero-mean white noise vector with $\boldsymbol{R}1$ covariance matrix. $\boldsymbol{h}1[\boldsymbol{x}(k), k]$ in Eq.(8) is a nonlinear transition function.

To apply extended Kalman filtering, the Jacobian matrices with respect to state vector should be worked out (Farrell and Barth, 1999). The transition function Jacobian matrix of the process model is an identity matrix, the Jacobian $\boldsymbol{H}1$ ("1" means the index of EKF1) of $\boldsymbol{h}1$ of the measurement model is presented by the following equation:

$$\boldsymbol{H}1[\hat{\boldsymbol{x}}(k+1|k),k]=\left.\frac{\partial \boldsymbol{h}1(\boldsymbol{x},k)}{\partial \boldsymbol{x}}\right|_{\boldsymbol{x}=\hat{\boldsymbol{x}}(k+1|k)}. \tag{9}$$

Details can be found in Appendix A.

EKF1 works in the following steps:

Step 1: State prediction and measurement prediction

$$\hat{\boldsymbol{x}}(k+1|k)=\boldsymbol{x}(k|k),$$
$$\boldsymbol{P}1(k+1|k)=\hat{\boldsymbol{x}}(k|k)\boldsymbol{P}1(k|k)\ \hat{\boldsymbol{x}}(k|k)+\boldsymbol{Q}1(k),$$
$$\hat{\boldsymbol{z}}(k+1|k)=\boldsymbol{h}1[\hat{\boldsymbol{x}}(k+1|k),k],$$
$$\boldsymbol{S}(k+1|k)=\boldsymbol{H}1[\hat{\boldsymbol{x}}(k+1|k),k]\times\boldsymbol{P}1(k+1|k)\boldsymbol{H}1^{\mathrm{T}}[\hat{\boldsymbol{x}}(k+1|k),k]+\boldsymbol{R}1(k).$$

Step 2: Compute EKF gain

$$\boldsymbol{K}(k+1|k)=\boldsymbol{P}1(k+1|k)\boldsymbol{H}1^{\mathrm{T}}[\hat{\boldsymbol{x}}(k+1|k),k]\boldsymbol{S}(k+1)^{-1}.$$

Step 3: Update estimate

$$\hat{\boldsymbol{x}}(k+1|k+1)=\hat{\boldsymbol{x}}(k+1|k)+\boldsymbol{K}(k+1)[\boldsymbol{z}(k+1)-\hat{\boldsymbol{z}}(k+1|k)],$$
$$\boldsymbol{P}1(k+1|k+1)=\boldsymbol{P}1(k+1|k)-\boldsymbol{K}(k+1)\boldsymbol{S}(k+1)\boldsymbol{K}^{\mathrm{T}}(k+1).$$

Repeat the above process for k=0, 1, …

In EKF2, the state vector is $[x, y, \psi]^{\mathrm{T}}$, and the estimation results of EKF1 are taken as the control input here. The estimate error covariance $\boldsymbol{P}1$ of EKF1 is used to determine the initial error covariance of the process model. The process model of EKF2 is:

$$\boldsymbol{x}(k+1)=\boldsymbol{f}2[\boldsymbol{x}(k),k]+\boldsymbol{w}(k), \tag{10}$$

where, $\boldsymbol{f}2[\boldsymbol{x}(k),k]$ is of the form of Eq.(1), $\boldsymbol{w}$ is the error vector of the process model with zero-mean and $\boldsymbol{Q}2$ the error covariance. Eqs.(11) and (12) are the measurement modes of the EKF2. The measurement vector $\boldsymbol{z}$ is directly recorded data from GPS positioning information with zero-mean and $\boldsymbol{R}2$ error covariance.

$$\boldsymbol{z}(k)=\boldsymbol{h}2[\boldsymbol{x}(k),k]+\boldsymbol{v}(k), \tag{11}$$

$$h_1(k)=x_1(k)=x(k),\quad h_2(k)=x_2(k)=y(k). \tag{12}$$

Jacobian matrix $\boldsymbol{F}2$ of transition function vector $\boldsymbol{f}2$ with respect to state vector and Jacobian matrix $\boldsymbol{H}2$ of transition function vector $\boldsymbol{h}2$ with respect to state vector are presented in the following forms respectively:

$$\boldsymbol{F}2=\left.\frac{\partial \boldsymbol{f}2(\boldsymbol{x},k)}{\partial \boldsymbol{x}}\right|_{\boldsymbol{x}=\hat{\boldsymbol{x}}(k|k)}=\begin{bmatrix}1 & 0 & -v\sin[\psi(k)+\beta(k)]\\ 0 & 1 & v\cos[\psi(k)+\beta(k)]\\ 0 & 0 & 1\end{bmatrix}, \tag{13}$$

$$\boldsymbol{H}2[\hat{\boldsymbol{x}}(k+1|k),k]=\left.\frac{\partial \boldsymbol{h}2(\boldsymbol{x},k)}{\partial \boldsymbol{x}}\right|_{\boldsymbol{x}=\hat{\boldsymbol{x}}(k+1|k)}=\begin{bmatrix}1 & 0 & 0\\ 0 & 1 & 0\end{bmatrix}. \tag{14}$$

EKF2 works in the following steps:

Step 1: State prediction and measurement prediction

$$\hat{\boldsymbol{x}}(k+1|k)=\boldsymbol{f}2(k|k),$$
$$\boldsymbol{P}2(k+1|k)=\boldsymbol{F}2(k|k)\boldsymbol{P}2(k|k)\boldsymbol{F}2^{\mathrm{T}}(k|k)+\boldsymbol{Q}1(k),$$
$$\hat{\boldsymbol{z}}(k+1|k)=\boldsymbol{h}2[\hat{\boldsymbol{x}}(k+1|k),k],$$
$$\boldsymbol{S}(k+1|k)=\boldsymbol{H}2[\hat{\boldsymbol{x}}(k+1|k),k]\times\boldsymbol{P}2(k+1|k)\boldsymbol{H}2^{\mathrm{T}}[\hat{\boldsymbol{x}}(k+1|k),k]+\boldsymbol{R}2(k).$$

Step 2: Compute EKF gain

$$\boldsymbol{K}(k+1|k)=\boldsymbol{P}2(k+1|k)\boldsymbol{H}2^{\mathrm{T}}[\hat{\boldsymbol{x}}(k+1|k),k]\boldsymbol{S}(k+1)^{-1}.$$

Step 3: Update estimate

$$\hat{\boldsymbol{x}}(k+1|k+1)=\hat{\boldsymbol{x}}(k+1|k)+\boldsymbol{K}(k+1)[\boldsymbol{z}(k+1)-\hat{\boldsymbol{z}}(k+1|k)],$$
$$\boldsymbol{P}2(k+1|k+1)=\boldsymbol{P}2(k+1|k)-\boldsymbol{K}(k+1)\boldsymbol{S}(k+1)\boldsymbol{K}^{\mathrm{T}}(k+1).$$

Repeat the above process for k=0, 1, …

By fusing the data from encoders and GPS, the position and orientation of the vehicle can be estimated using the above process. Although one kind of sensor data only, i.e., GPS measurement is used explicitly in EKF2, we note that EKF2 takes the vehicle velocity and sideslip angle, which are estimation outputs in EKF1, as its control inputs. So, actually EKF2 indirectly fuses measurement from six encoders with data from GPS sensor. The estimation by EKF2 can achieve high accuracy due to the high accuracy data from RTK of GPS.

RTK, i.e., Real-Time Kinematics, can give centimeter-level accuracy. The GPS receivers used in RTK systems should be dual-frequency types that use standard code and carrier phase GPS signals, and track the second carrier phase signal that enable RTK GPS receivers to lock into the high accuracy (centimeter level). But, high accuracy needs more requirements, for example, to get initialized, RTK needs a minimum of five satellites, after that it can operate with four (DGPS needs a minimum of three for sub-meter accuracy). Furthermore, for RTK, GPS receiver must be capable of On-the-Fly initialization (obtaining centimeter accuracy while moving). A RTK GPS receiver (Trimble, MS750) is installed on our Cycab. Fig.4 shows a scenario of RTK GPS positioning system. There are two GPS receivers being used, one is for base station, and the other is for rover, e.g. our Cycab. Generally the rover receiver has two operation modes, e.g., fixed RTK (centimeter accuracy), DGPS (sub-meter accuracy). Between the two modes is a transient mode, i.e., float RTK, which has better accuracy than DGPS, but worse accuracy than fixed RTK.

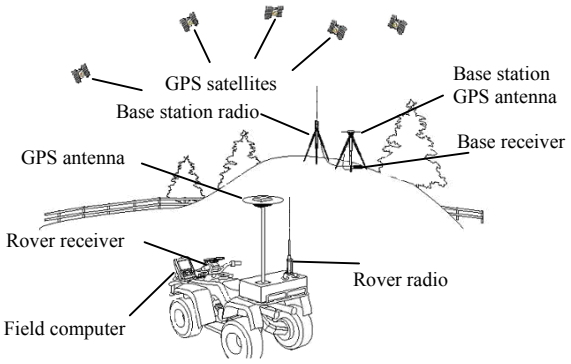

Fig.4 A scenario of RTK GPS positioning system

However, in practice, fixed RTK mode is not constantly available during the vehicle driving. There are many cases that could result in satellites signals mask or deterioration, for example, the vehicle passing by a bridge or high building, or being close to a high tree, etc. Even at a nearly open-view site, the deterioration of GPS signals could occur due to ionosphere activities or satellites failure. In such cases, GPS operation mode would be degraded from Fixed RTK to Float RTK or even DGPS (We will not discuss the situations of completely losing GPS signals or degrading to standard GPS in this paper), the estimation precision also will deteriorate significantly as well. To compensate for the lost precision as much as possible, dead reckoning is applied to replace EKF2 to produce the position and orientation of the vehicle during the above deterioration stages. The dead reckoning here is a Runga-Kutta-based algorithm to solve the differential Eq.(10).

Arbitration mechanism

To choose the best estimate outputs from EKF2 or the dead-reckoning, an arbitrator (Fig.5) is designed to determine which estimate is online. In the NMEA data output of the GPS rover receiver is a

message segment of "GPS quality indicator", which indicates the current GPS modes by digits. The arbitrator utilizes such messages to switch the algorithms between EKF2 and Runga-Kutta-based dead reckoning. Fig.5 shows that, the dead reckoning has to subject to timeout checking, its "lifespan" is limited to a preset interval. Or else, the drift of encoders through time could go beyond a specified error bound, even beyond the error bound of DGPS or float RTK.

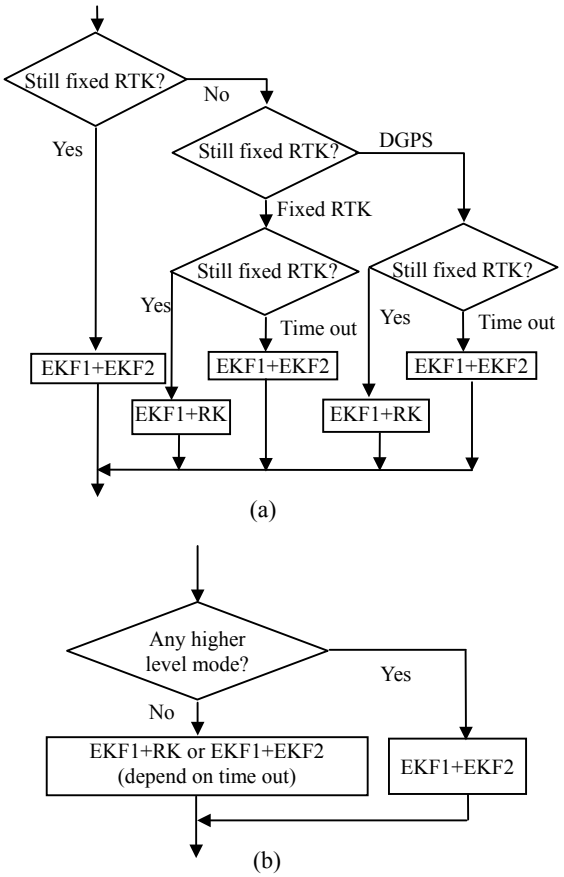

Fig.5 Arbitration mechanism. (a) Arbitration when vehicle runs in fixed RTK mode; (b) Arbitration when vehicle runs in non-RTK (fixed) mode

Another issue is that the dead reckoning must be initialized by the latest estimation results. In other words, the dead reckoning should be calibrated by the latest available GPS data before it is put into service.

EXPERIMENTAL RESULTS

Experiments were carried out in a car park with some low trees and houses nearby. In most cases, the rover GPS receiver on our vehicle works in fixed RTK mode.

Estimation outputs of EKF1 are shown in Fig.6, estimation results can rapidly converge, even initializing the state vector with some bias. To evaluate the estimation, a quasi-true velocity by post-processing

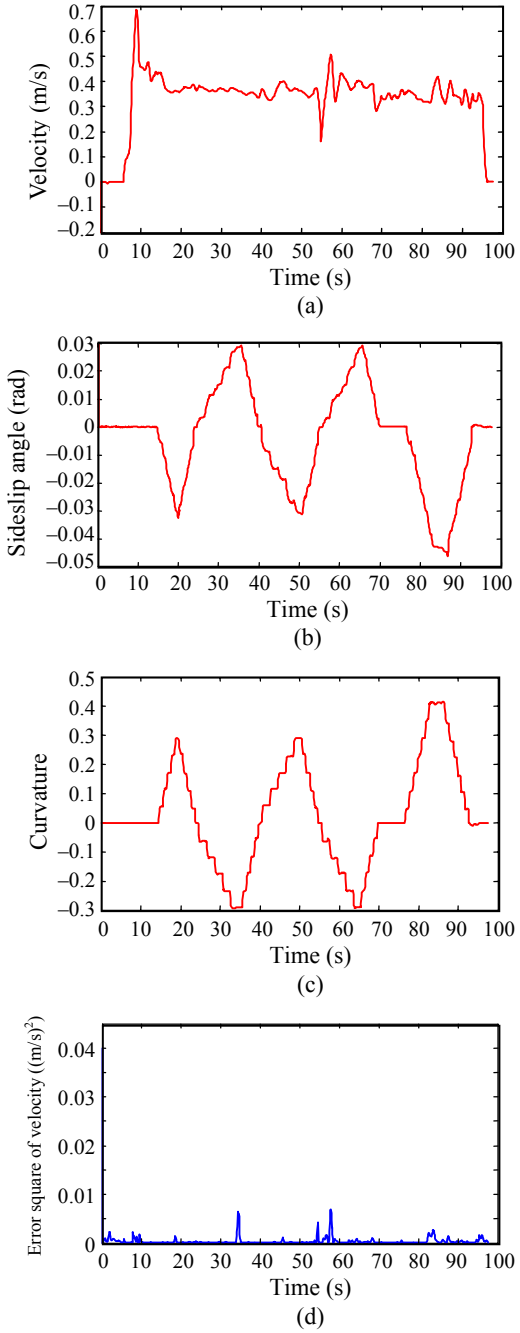

Fig.6 Results of EKF1. (a) Velocity by EKF1; (b) Sideslip angle by EKF1; (c) Curvature by EKF1; (d) Square error of velocity

of GPS data is used for comparison; the square error shown in Fig.6d reflects the performance of estimation to some extent.

Fig.7 shows the trajectories of two experiments that basically represent the cases that most possibly occur when the vehicle is running at a nearly open-view site.

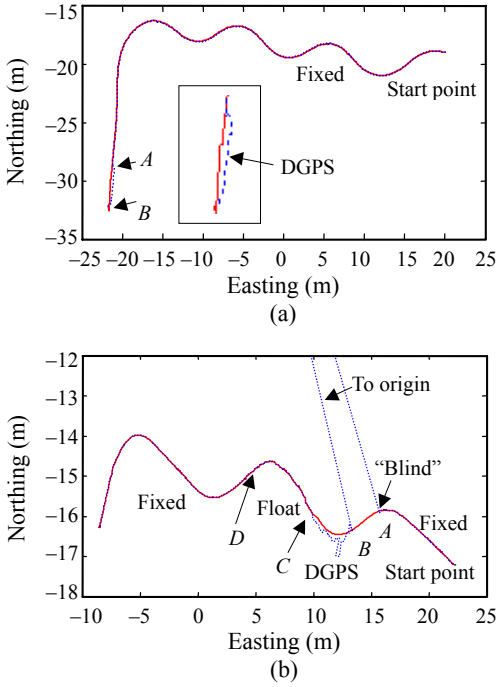

Fig.7 Trajectories by EKF (solid line) and GPS only (dotted line). (a) Experiment 1; (b) Experiment 2

In Experiment 1, the vehicle starts running from the upper right side of Fig.7a with GPS working in fixed RTK mode. The dotted line is the trajectory recorded by GPS data, the solid line is produced by the estimator represented in Fig.2. The estimation mostly coincides with the one by GPS, because EKF1+EKF2 is being used to estimate the states according to the arbitration mechanism. From the starting point, GPS is in fixed RTK mode; good results are produced by EKF1+EKF2. When the vehicle reaches segment *AB*, the DGPS mode occurs and a significant error (magnified profile is shown in the right window) emerges accordingly. Thus RTK1+RK algorithm is carried out within the timeout period (15 s for DGPS, 20 s for RTK Float). The upper little arrow *A* points to the entering DGPS epoch, the lower arrow *B* points to the recovering to fixed RTK epoch. Clearly the estimation of EKF1+RK is quite good in such case. GPS works in fixed RTK mode again in the last period (after point *B*), the estimator applies EKF1+EKF2 accordingly.

Experiment 2 presents a worse situation of GPS signal (Fig.7b). A signal block occurs when the antenna of the rover receiver is intentionally covered for a short term. This experiment was aimed at showing the performance of the estimator when the GPS works under bad conditions. The vehicle starts running with GPS working in fixed RTK mode, EKF1+EKF2 is used to estimate the states. From point *A*, the GPS signal is lost suddenly, there is no normal position data output (in such case, zeros are taken as the position output, so the dotted line jumps to the origin), GPS receiver is in the "blind" status. At the point *B*, the GPS signal recovers, enters the DGPS mode first, then enters the float RTK mode at point *C*, finally returns to the high precise mode, i.e., fixed RTK at point *D*. From point *B* to point *D*, a typical complete RTK initialization procedure is performed, which takes about 30 s. From point *A*, the EKF1+RK (dead reckoning) is switched on to estimate the configuration of the vehicle. In this case, the dead reckoning only lasts 15 s under the rule of the arbitrator. After the timeout, the estimator has to switch to EKF1+EKF2 at around the point *C* due to the drift of the encoders.

LIMITATIONS

This paper's proposed approach has some limitations, especially the problem of our not being sure that the GPS signal is always good enough in practice, would seriously and adversely impact the performance of the vehicle's navigation system. And, although using data from six encoders and Runga-Kutta-based dead reckoning we can work out the vehicle position and orientation, error accumulation would get large when fixed RTK mode is lost for a long term. So, positioning and navigation cannot completely rely on only one kind of sensor (encoder). If RTK GPS is not available, more sensors, such as gyroscope, accelerometer, digital compass, etc. should be installed on the vehicle. In our future research we will mount an IMU (inertial measurement unit) and laser scanner on Cycab, fuse them with encoders and GPS into EKF architecture to offer better and more reliable estimation.

CONCLUSION

Real-time kinematics positioning of GPS provides very high precision (centimeter-level) for navigation of vehicles or outdoor mobile robots. But to be practical, it has to be used together with other sensors if deterioration of GPS signals is considered. In this paper, a 4WS vehicle is considered and we propose an estimator consisting of two extended Kalman filters, a Runga-Kutta-based dead reckoning unit and an arbitrator to estimate the position and orientation of the vehicle. Results of experiments showed the efficiency and high accuracy of estimation, especially for the cases of short-term deterioration of satellites signals.

References

Abbott, E., Powell, D., 1999. Land-vehicle navigation using GPS. *Proceeding of IEEE*, **87**(1):145-162.

Farrell, J.A., Barth, M., 1999. The Global Positioning System and Inertial Navigation. McGraw-Hill.

Iida, M., Kudou, M., Ono, O., Umeda, M., 2000. Automatic Following Control for Agricultural Vehicle. AMC, Nagoya, p.158-162.

Kobayashi, K., Watanabe, K., 1994. Accurate Navigation via Sensor Fusion of Differential GPS and Rate-Gyro. IMTC, Hamamatsu, p.556-559.

Lee, M., 1997. Arrier-Phase Differential GPS for Automatic Control of Land Vehicles. Ph.D Thesis, Stanford University.

Tay, E.K., 1999. Modeling, Analysis and Control Design for an Automated Guided Vehicle. MS Thesis, Nanyang Tech. Univ.

Wang, D., Tay, E.K., Zribi, M., 1998. Modeling of an AGV for Handling Heavy Containers. The 3rd International Conference on Advanced Mechatronics, Japan, p.67-72.

APPENDIX A

Supposing,

$$A_{\mathrm{f}}(k)=\sqrt{l_{\mathrm{f}}{}^2\rho^2+2l_{\mathrm{f}}\rho\sin\beta+1},$$

$$A_{\mathrm{r}}(k)=\sqrt{l_{\mathrm{r}}{}^2\rho^2-2l_{\mathrm{r}}\rho\sin\beta+1},$$

$$B_{\mathrm{f}}(k)=(-\cos\beta+\sqrt{l_{\mathrm{f}}{}^2\rho^2+2l_{\mathrm{f}}\rho\sin\beta+1})\Big/(l_{\mathrm{f}}\rho+\sin\beta),$$

$$B_{\mathrm{f}}(k)=(\cos\beta-\sqrt{l_{\mathrm{f}}{}^2\rho^2-2l_{\mathrm{f}}\rho\sin\beta+1})\Big/(l_{\mathrm{f}}\rho-\sin\beta),$$

$$C_{+}=1+\frac{b\rho}{\cos\beta},\ C_{-}=1-\frac{b\rho}{\cos\beta},$$

$$D_{\mathrm{f}}=1-B_{\mathrm{f}}{}^2,\ D_{\mathrm{r}}=1-B_{\mathrm{r}}{}^2,$$

$$E_{\mathrm{f}-}=l_{\mathrm{f}}\rho-\sin\beta,\ E_{\mathrm{f}+}=l_{\mathrm{f}}\rho+\sin\beta,$$

$$E_{\mathrm{r}-}=l_{\mathrm{r}}\rho-\sin\beta,\ E_{\mathrm{r}+}=l_{\mathrm{r}}\rho+\sin\beta.$$

The Jacobian matrix of the EKF1 is

$$\boldsymbol{H}1[\hat{\boldsymbol{x}}(k+1\,|\,k),k]=\frac{\partial \boldsymbol{h}1(\boldsymbol{x},k)}{\partial \boldsymbol{x}}\bigg|_{\boldsymbol{x}=\hat{\boldsymbol{x}}(k+1|k)}=$$

$$\begin{bmatrix}
\partial v_{\mathrm{fl}}/\partial v & \partial v_{\mathrm{fl}}/\partial\beta & \partial v_{\mathrm{fl}}/\partial\rho\\
\partial v_{\mathrm{fr}}/\partial v & \partial v_{\mathrm{fr}}/\partial\beta & \partial v_{\mathrm{fr}}/\partial\rho\\
\partial v_{\mathrm{rl}}/\partial v & \partial v_{\mathrm{rl}}/\partial\beta & \partial v_{\mathrm{rl}}/\partial\rho\\
\partial v_{\mathrm{rr}}/\partial v & \partial v_{\mathrm{rr}}/\partial\beta & \partial v_{\mathrm{rr}}/\partial\rho\\
\partial\tan(\delta_{\mathrm{f}}/2)/\partial v & \partial\tan(\delta_{\mathrm{f}}/2)/\partial\beta & \partial\tan(\delta_{\mathrm{f}}/2)/\partial\rho\\
\partial\tan(\delta_{\mathrm{r}}/2)/\partial v & \partial\tan(\delta_{\mathrm{r}}/2)/\partial\beta & \partial\tan(\delta_{\mathrm{r}}/2)/\partial\rho
\end{bmatrix},$$

where,

$$\partial v_{\mathrm{fl}}/\partial v=\cos\beta\sqrt{C_{-}{}^2+4B_{\mathrm{f}}{}^2/D_{\mathrm{f}}{}^2},$$

$$\partial v_{\mathrm{fr}}/\partial v=\cos\beta\sqrt{C_{+}{}^2+4B_{\mathrm{f}}{}^2/D_{\mathrm{f}}{}^2},$$

$$\partial v_{\mathrm{fl}}/\partial\beta=v\cos\beta\left\{(C_{+}{}^2+4B_{\mathrm{f}}{}^2/D_{\mathrm{f}}{}^2)^{-1/2}\left(\frac{bC_{+}}{\cos\beta}-\frac{4B_{\mathrm{f}}l_{\mathrm{f}}}{D_{\mathrm{f}}{}^2A_{\mathrm{f}}}-\frac{4B_{\mathrm{f}}{}^2l_{\mathrm{f}}}{D_{\mathrm{f}}{}^2E_{\mathrm{f}-}}-\frac{8B_{\mathrm{f}}{}^3l_{\mathrm{f}}E_{\mathrm{f}-}+8B_{\mathrm{f}}{}^4l_{\mathrm{f}}A_{\mathrm{f}}}{D_{\mathrm{f}}E_{\mathrm{f}-}A_{\mathrm{f}}}\right)\right\},$$

$$\partial v_{\mathrm{fl}}/\partial\rho=v\cos\beta\left\{(C_{+}{}^2+4B_{\mathrm{f}}{}^2/D_{\mathrm{f}}{}^2)^{-1/2}\left(-\frac{bC_{-}}{\cos\beta}+\frac{4B_{\mathrm{f}}l_{\mathrm{f}}}{D_{\mathrm{f}}{}^2A_{\mathrm{f}}}-\frac{4B_{\mathrm{f}}{}^2l_{\mathrm{f}}}{D_{\mathrm{f}}{}^2E_{\mathrm{f}-}}+\frac{8B_{\mathrm{f}}{}^3l_{\mathrm{f}}E_{\mathrm{f}-}-8B_{\mathrm{f}}{}^4l_{\mathrm{f}}A_{\mathrm{f}}}{D_{\mathrm{f}}E_{\mathrm{f}-}A_{\mathrm{f}}}\right)\right\},$$

$$\partial v_{\mathrm{fr}}/\partial\beta=-v\sin\beta\sqrt{C_{+}{}^2+4B_{\mathrm{f}}{}^2/D_{\mathrm{f}}{}^2}+v\cos\beta\left\{(C_{+}{}^2+4B_{\mathrm{f}}{}^2/D_{\mathrm{f}}{}^2)^{-1/2}\left(\frac{b\rho C_{+}\sin\beta}{\cos^2\beta}+\frac{4B_{\mathrm{f}}(\sin\beta+l_{\mathrm{f}}\rho\cos\beta/A_{\mathrm{f}})-4B_{\mathrm{f}}{}^2\cos\beta}{E_{\mathrm{f}+}D_{\mathrm{f}}{}^2}+\frac{8B_{\mathrm{f}}{}^3(\sin\beta+l_{\mathrm{f}}\rho\cos\beta/A_{\mathrm{f}}-B_{\mathrm{f}}\cos\beta)}{E_{\mathrm{f}+}D_{\mathrm{f}}}\right)\right\},$$

$$\partial v_{\mathrm{fr}}/\partial\rho=v\cos\beta\left\{(C_{+}{}^2+4B_{\mathrm{f}}{}^2/D_{\mathrm{f}}{}^2)^{-1/2}\left(\frac{bC_{+}}{\cos^2\beta}+\frac{4B_{\mathrm{f}}l_{\mathrm{f}}}{A_{\mathrm{f}}D_{\mathrm{f}}{}^2}-\frac{4B_{\mathrm{f}}{}^2l_{\mathrm{f}}}{E_{\mathrm{f}+}D_{\mathrm{f}}{}^2}+\frac{8B_{\mathrm{f}}{}^3l_{\mathrm{f}}E_{\mathrm{f}+}+8B_{\mathrm{f}}{}^4l_{\mathrm{f}}A_{\mathrm{f}}}{E_{\mathrm{f}+}D_{\mathrm{f}}A_{\mathrm{f}}}\right)\right\},$$

$$\partial v_{\mathrm{rl}}/\partial v=\cos\beta\sqrt{C_{-}^{\ 2}+4B_{\mathrm{r}}^{\ 2}/D_{\mathrm{r}}^{\ 2}},$$

$$\partial v_{\mathrm{rr}}/\partial v=\cos\beta\sqrt{C_{+}^{\ 2}+4B_{\mathrm{r}}^{\ 2}/D_{\mathrm{r}}^{\ 2}},$$

$$\partial v_{\mathrm{rl}}/\partial\beta=-v\sin\beta\sqrt{C_{-}^{\ 2}+4B_{\mathrm{r}}^{\ 2}/D_{\mathrm{r}}^{\ 2}}+v\cos\beta\left\{(C_{-}^{\ 2}+4B_{\mathrm{r}}^{\ 2}/D_{\mathrm{r}}^{\ 2})^{-1/2}\left(-\frac{bC_{-}\rho\sin\beta}{\cos^{2}\beta}+\frac{4B_{\mathrm{r}}(-\sin\beta+l_{\mathrm{r}}\rho\cos\beta/A_{\mathrm{r}})+4B_{\mathrm{r}}^{\ 2}\cos\beta}{D_{\mathrm{r}}^{\ 2}E_{\mathrm{r}-}}+\frac{8B_{\mathrm{r}}^{\ 3}(-\sin\beta+l_{\mathrm{r}}\rho\cos\beta/A_{\mathrm{r}}+B_{\mathrm{r}}\cos\beta)}{D_{\mathrm{r}}E_{\mathrm{r}-}}\right)\right\},$$

$$\partial v_{\mathrm{rl}}/\partial\rho=v\cos\beta\left\{(C_{-}^{\ 2}+4B_{\mathrm{r}}^{\ 2}/D_{\mathrm{r}}^{\ 2})^{-1/2}\left(-\frac{bC_{-}}{\cos\beta}-\frac{4B_{\mathrm{r}}l_{\mathrm{r}}}{D_{\mathrm{r}}^{\ 2}A_{\mathrm{r}}}-\frac{4B_{\mathrm{r}}^{\ 2}l_{\mathrm{r}}}{D_{\mathrm{r}}^{\ 2}E_{\mathrm{r}-}}+\frac{-8B_{\mathrm{r}}^{\ 3}l_{f}E_{\mathrm{r}+}-8B_{\mathrm{r}}^{\ 4}l_{\mathrm{r}}A_{\mathrm{r}}}{D_{\mathrm{r}}E_{\mathrm{r}-}A_{\mathrm{r}}}\right)\right\},$$

$$\partial v_{\mathrm{rr}}/\partial\beta=-v\sin\beta\sqrt{C_{+}^{\ 2}+4B_{\mathrm{r}}^{\ 2}/D_{\mathrm{r}}^{\ 2}}+v\cos\beta\left\{(C_{+}^{\ 2}+4B_{\mathrm{f}}^{\ 2}/D_{\mathrm{f}}^{\ 2})^{-1/2}\left(\frac{b\rho C_{+}\sin\beta}{\cos^{2}\beta}+\frac{4B_{\mathrm{r}}(-\sin\beta+l_{\mathrm{r}}\rho\cos\beta/A_{\mathrm{r}})+4B_{\mathrm{r}}^{\ 2}\cos\beta}{E_{\mathrm{r}-}D_{\mathrm{r}}^{\ 2}}+\frac{8B_{\mathrm{r}}^{\ 3}(-\sin\beta+l_{\mathrm{r}}\rho\cos\beta/A_{\mathrm{r}}+B_{\mathrm{r}}\cos\beta)}{E_{\mathrm{r}-}D_{\mathrm{r}}}\right)\right\},$$

$$\partial v_{\mathrm{rr}}/\partial\rho=v\cos\beta\left\{(C_{+}^{\ 2}+4B_{\mathrm{r}}^{\ 2}/D_{\mathrm{r}}^{\ 2})^{-1/2}\left(\frac{bC_{+}}{\cos\beta}-\frac{4B_{\mathrm{f}}l_{\mathrm{f}}}{A_{\mathrm{r}}D_{\mathrm{r}}^{\ 2}}-\frac{4B_{\mathrm{r}}^{\ 2}l_{\mathrm{r}}}{E_{\mathrm{r}-}D_{\mathrm{r}}^{\ 2}}+\frac{-8B_{\mathrm{r}}^{\ 3}l_{\mathrm{r}}E_{\mathrm{r}-}-8B_{\mathrm{r}}^{\ 4}l_{\mathrm{r}}A_{\mathrm{r}}}{E_{\mathrm{r}-}D_{\mathrm{r}}A_{\mathrm{r}}}\right)\right\},$$

$$\partial\tan(\delta_{\mathrm{f}}/2)/\partial v=0,$$

$$\partial\tan(\delta_{\mathrm{f}}/2)/\partial\beta=\frac{\sin\beta+l_{\mathrm{f}}\rho\cos\beta/A_{\mathrm{f}}}{E_{\mathrm{f}+}}+\frac{B_{\mathrm{f}}\cos\beta}{E_{\mathrm{f}+}},$$

$$\partial\tan(\delta_{\mathrm{f}}/2)/\partial\rho=\frac{l_{\mathrm{f}}}{A_{\mathrm{f}}}-\frac{B_{\mathrm{f}}l_{\mathrm{f}}}{E_{\mathrm{f}+}},$$

$$\partial\tan(\delta_{\mathrm{r}}/2)/\partial v=0,$$

$$\partial\tan(\delta_{\mathrm{r}}/2)/\partial\beta=\frac{-\sin\beta+l_{\mathrm{r}}\rho\cos\beta/A_{\mathrm{r}}}{E_{\mathrm{r}-}}+\frac{B_{\mathrm{r}}\cos\beta}{E_{\mathrm{r}-}},$$

$$\partial\tan(\delta_{\mathrm{r}}/2)/\partial\rho=\frac{l_{\mathrm{r}}}{A_{\mathrm{r}}}-\frac{B_{\mathrm{r}}l_{\mathrm{r}}}{E_{\mathrm{r}-}}.$$